C. R. Chimie 22 (2019) 3–12

Contents lists available at ScienceDirect

Comptes Rendus Chimie

www.sciencedirect.com

Full paper/Mémoire

Synthesis, crystal structure, and density functional theory study of a zinc(II) complex containing terpyridine and pyridine-2,6-dicarboxylic acid ligands: Analysis of the interactions with amoxicillin

Adedibu C. Tella [a, **], Joshua A. Obaleye [a], Margaret D. Olawale [b], Jean Marie Vianney Ngororabanga [c], Adeniyi S. Ogunlaja [c, *], Susan A. Bourne [d]

[a] Department of Chemistry, P.M.B. 1515, University of Ilorin, Ilorin, Kwara State, Nigeria
[b] Department of Chemical and Physical Sciences, Elizade University, Ilara Mokin, Ondo State, Nigeria
[c] Department of Chemistry, Nelson Mandela University, PO Box 77000, Port Elizabeth, 6031, South Africa
[d] Centre for Supramolecular Chemistry Research, Department of Chemistry, University of Cape Town, Rondebosch 7701, South Africa

ARTICLE INFO

Article history:
Received 14 September 2018
Accepted 13 November 2018
Available online 19 December 2018

Keywords:
Crystal structure
Amoxicillin
Luminescence
DFT calculations

ABSTRACT

An octahedral zinc(II) complex of 2,2′:6′,2″-terpyridine (Tpy) and pyridine-2,6-dicarboxylate (Pydc), [Zn(II)(Tpy)(Pydc)·4H_2O] was synthesized and its structure was determined by a single-crystal X-ray diffraction. The ligand pyridine-2,6-dicarboxylate coordinated to the zinc(II) ion via two pairs of carboxylate oxygens and one nitrogen atom, whereas 2,2′:6′,2″-terpyridine also contributed three coordination bonds through its nitrogen atoms. [Zn(II)(Tpy)(Pydc)·4H_2O] showed luminescence properties between 412 and 435 nm in DMSO. The solid-state octahedral geometry of [Zn(II)(Tpy)(Pydc)·4H_2O] was also preserved in solution as confirmed by the observed UV λ_{ex} = 346. Experimental and theoretical studies indicated that [Zn(II)(Tpy)(Pydc)·4H_2O] interacted with amoxicillin. Density functional theory calculations at B3LYP/LanL2dz level of theory suggested that [Zn(II)(Tpy)(pydc)·4H_2O] dimer interacts with (2*S*,5*R*,6*R*)-6-{[(2*R*)-2-amino-2-(4-hydroxyphenyl)-acetyl]amino}-3,3-dimethyl-7-oxo-4-thia-1-azabicyclo[3.2.0]heptane-24-carboxylic acid (amoxicillin) via highest occupied molecular orbital and lowest unoccupied molecular orbital, π–π interaction, hydrogen bond interaction, and van der Waals forces, thus influencing [Zn(II)(Tpy)(Pydc)·4H_2O] properties.

1. Introduction

Metal complexes are important and have found applications in different fields such as catalysis, biology, and material sciences [1–4]. These complexes may have different geometries; therefore, they are potentially biologically active [5]. Metal complexes such as Cu(II), Zn(II), Ni(II), and Co(II) have been studied extensively because of their attractive chemical and physical properties [6,7]. Copper, nickel, cobalt, and zinc are sometimes called biometals because they help catalyze biochemical processes in humans [8].

Lapshin and Alekseev [9] reported that biometals such as copper ions form stable complexes in the human body upon simultaneous administration of metal-containing vitamins and antibiotics such as ampicillin, amoxicillin, and cephalexin as most contain an amino group [10]. These antibiotics promote the removal of metals such as copper from the body, whereas the metal also catalyzes the

* Corresponding author.
** Corresponding author.
E-mail addresses: ac_tella@yahoo.co.uk (A.C. Tella), adeniyi.ogunlaja@mandela.ac.za (A.S. Ogunlaja).

https://doi.org/10.1016/j.crci.2018.11.007
1631-0748/

hydrolysis of antibiotics, and this can reduce the effect of antimicrobial therapy [10]. Strachunskii and Kozlov confirmed that Zn(II) mediates vancomycin (a natural product glycopeptide antibiotic) polymerization, thereby enhancing its binding affinity toward D-Ala-D-Lac precursors [11].

To the best of our knowledge this is the first study to report that zinc(II) complex of 2,2′:6′,2″-terpyridine (Tpy) and pyridine-2,6-dicarboxylic acid (Pydc) has been prepared and its interaction with antibiotics has been studied. The objective of this work was to present the synthesis and theoretical study on electronic and molecular structure of the zinc(II) complex of 2,2′:6′,2″-terpyridine (Tpy) and pyridine-2,6-dicarboxylic acid (Pydc), [Zn(II)(Tpy)(Pydc)·$4H_2O$] and to determine relationship between the molecular structure of the compound and theoretical interaction efficiency with amoxicillin. We studied the interaction of [Zn(II)(Tpy)(Pydc)·$4H_2O$] and amoxicillin theoretically to examine how the nature of a central metal ion influences the geometry and electronic characteristics (electrostatic potential and spin density distribution, highest occupied molecular orbital (HOMO), and lowest unoccupied molecular orbital (LUMO) structure), the absolute electronegativity (χ) values, and the fraction of electrons transferred (ΔN) between metal complexes and amoxicillin.

2. Experimental section

2.1. Materials and physical measurements

Chemicals and solvents were acquired from Sigma–Aldrich Company and used without further purification. Fourier transform infrared (FT-IR) and elemental analyses of [Zn(II)(Tpy)(Pydc)·$4H_2O$] were determined using a PerkinElmer spectrophotometer and PerkinElmer CHN analyzer 2400 series II, respectively. Thermogravimetric analysis (TGA) was carried out using TA Instruments TA-Q500 under dry nitrogen gas at a flow rate of 60 $cm^3\ min^{-1}$. Samples with a mass in the range of 1–5 mg were placed in an open platinum crucible and heated at a rate of 10 °C min^{-1}.

2.1.1. Crystallographic data collection and structural analysis

Single crystals suitable for X-ray crystallography were obtained by slow evaporation of aqueous/alcoholic solution. Details of the crystal parameters, data collection, and refinements are listed in Table 1. Data were collected using a Bruker KAPPA Apex II Dual Source diffractometer with graphite-monochromated Mo Kα ($\lambda = 0.71073$ Å) radiation at 293 K. The structure was solved by direct methods in SHELXS and refined by full-matrix least-squares methods based on F^2 using SHELXL [12]. Table 2 lists selected molecular parameters.

2.2. Theory and computational detail

Density functional theory (DFT) methods were used in this study. All of the calculations were done by Gaussian 09 software [13], using the B3LYP functional [14,15] and a LanL2dz basis set. The B3LYP, a version of DFT method [16], uses Beche's three-parameter functional (B3) and includes a mixture of HF with DFT exchange terms associated with the gradient-corrected correlation functional of Lee, Yang, and Parr [14,15].

Molecular interactions between [Zn(II)(Tpy)(Pydc)·$4H_2O$] and amoxicillin were calculated at 298 K. Ab initio calculations such as HOMO energy (E_{HOMO}), LUMO energy (E_{LUMO}), LUMO–HOMO energy gap (ΔE), hardness (η), softness (σ), electronegativity (χ), and chemical potential

Table 1
Crystal data and structural refinement details of [Zn(II)(Tpy)(Pydc)·$4H_2O$].

Crystallographic data	[Zn(II)(Tpy)(Pydc)·$4H_2O$]
Empirical formula	$C_{22}H_{22}N_4O_4Zn$
Formula weight	535.81
Crystal system	Triclinic
Space group	$P\bar{1}$
a (Å)	8.431 (3)
b (Å)	12.696 (4)
c (Å)	21.701 (7)
α	85.465 (7)^0
β	84.808 (6)^0
γ	82.950 (7)^0
V (Å^3)	2290.6 (13)
Z	4
F (000)	1104
D_x (Mg m^{-3})	1.554
Diffraction radiation type	Mo Kα
λ (Å)	0.71073
μ (mm^{-1})	1.13
Crystal description	Needle
Temperature (K)	173
Crystal size (max × mid × min)	0.14 × 0.09 × 0.07
Measurement device	Bruker APEX II diffractometer
Absorption correction type	Multiscan
Radiation monochromator	Graphite
Radiation source	Fine focus sealed tube
No. of F values used [$I > 2\sigma(I)$]	6125
Index ranges $\pm h$, $\pm k$, $\pm l$	±10, ±16, ±27
No. of unique reflections	9878
R_{int}	0.096
Weighting expression w	$1/[\sigma^2(F_o^2) + (0.0585P)^2 + 1.1595P]$, where $P = (F_o^2 + 2F_c^2)/3$
T_{min}/T_{max} (absorption correction)	0.858/0.925
$R[F^2 > 2\sigma(F^2)]$	0.0554
$wR(F^2)$	1.1527
S (goodness of fit)	1.034
$(\Delta/\sigma)_{max}$ (refine_ls_shift/su_max)	0.000
Final $\Delta\rho_{max}/\Delta\rho_{min}$ (e Å^{-3})	0.64/−0.47

Table 2
Selected bond distances (Å) and angles (°) for [Zn(II)(Tpy)(Pydc)·$4H_2O$] (A) and [Zn(II)(Tpy)(Pydc)·$4H_2O$] (B).

Bond length (Å)/angles	A	B
Zn–N27	2.030 (3)	2.020 (3)
Zn–N12	2.072 (3)	2.065 (3)
Zn–O30	2.138 (3)	2.180 (3)
Zn–N1	2.173 (3)	2.161 (3)
Zn–N13	2.173 (3)	2.161 (3)
Zn–O19	2.268 (3)	2.213 (3)
N27–Zn–N12	163.89 (13)	166.32 (13)
N27–Zn–O30	77.03 (12)	76.58 (12)
N12–Zn–O30	118.30 (12)	116.90 (12)
N27–Zn–N13	99.90 (13)	101.78 (13)
N12–Zn–N1	75.83 (13)	75.92 (13)
O30–Zn–O19	151.74 (11)	151.93 (11)

(μ), $I = -E_{HOMO}$, $A = -E_{LUMO}$ were calculated using the following equations:

$$\eta = \frac{I - A}{2} \quad (1)$$

$$\sigma = \frac{1}{\eta} \quad (2)$$

$$\chi = \frac{I + A}{2} \quad (3)$$

$$\mu = -\chi \quad (4)$$

Finally, LUMO–HOMO energy gap (ΔE) was calculated using the following formula: $\Delta E = E_{LUMO} - E_{HOMO}$.

2.3. Synthesis of [Zn(II)(Tpy)(Pydc)·4H2O]

The solvothermal synthesis of [Zn(II)(Tpy)(Pydc)·$4H_2O$] was performed by reacting a mixture of $Zn(NO_3)_2 \cdot 6H_2O$ (1.89 g, 0.01 mol), 2,2′:6′,2″-terpyridine (2.3 g, 0.01 mol), and pyridine-2,6-dicarboxylic acid (1.67 g, 0.01 mol), which had been dissolved in 30 mL mixture of water, ethanol, and methanol (1:1:1), respectively. The dissolved mixture was transferred into a reaction vessel in an oven and set to 160 °C for 5 days (Scheme 1). The reaction was slow-cooled gradually and left in the oven at room temperature for another 24 h to obtain colorless needles of [Zn(II)(Tpy)(Pydc)·$4H_2O$] (Scheme 1). Yield: 76%. CHN analysis; Anal Found (Calcd) % for $C_{22}H_{22}N_4O_8Zn$: C, 49.31 (49.24); H, 4.14 (4.08); N, 10.46 (10.44).

2.4. Interaction studies

For the experimental interaction studies, 0.05 g of [Zn(II)(Tpy)(Pydc)·$4H_2O$] was brought in contact with a 2 mL solution containing 5.47×10^{-3} M of 3.99 mg of amoxicillin (Sigma–Aldrich) dissolved in 0.2 mL DMSO, followed by adding 1.8 mL H_2O. The [Zn(II)(Tpy)(Pydc)·$4H_2O$] was separated from the resultant mixture via centrifugation at 2000 rpm for 5 min, and the resultant solution was analyzed using a UV–vis spectrophotometer at 256 nm at regular time intervals (every 30 min).

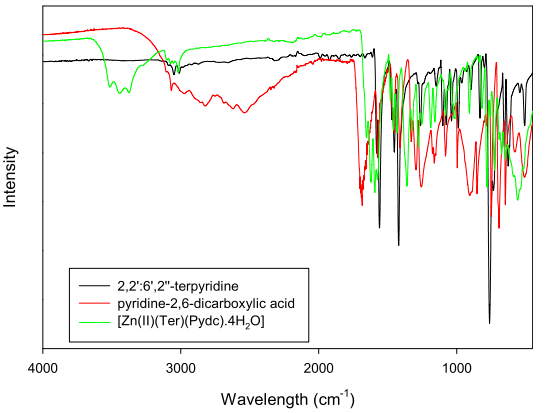

Fig. 1. FT-IR of spectrum of 2,2′:6′,2″-terpyridine, pyridine-2,6-dicarboxylic acid, and [Zn(II)(Tpy)(Pydc)·$4H_2O$].

3. Results and discussion

The crystal is clearly different in color as compared with any of the starting materials. Image of the colorless needle like crystals of [Zn(II)(Tpy)(Pydc)·$4H_2O$] is shown in Fig. S1.

3.1. FT-IR spectra

FT-IR of 2,2′:6′,2″-terpyridine, pyridine-2,6-dicarboxylic acid, and [Zn(II)(Tpy)(Pydc)·$4H_2O$] shows significant changes in absorption frequencies due to disappearance of some characteristic frequencies that occurred at coordination sites of 2,2′:6′,2″-terpyridine and pyridine-2,6-dicarboxylic acid upon complex formation (Fig. 1). Vibration frequencies at 1685, 3100, and 1585–1550 cm^{-1} were ascribed to ν(C=O), ν(O–H), and ν(C=N), respectively, for pyridine-2,6-dicarboxylic acid, whereas 2,2′:6′,2″-terpyridine displayed an interesting ν(C=N) frequency at around 1595–1550 cm^{-1}.

The characteristic absorption band –OH of pyridine-2,6-dicarboxylic acid at 3100 cm^{-1} disappeared upon coordination with Zn(II) salt [17]. With a formation of noncoordinated water molecules observed at 3454 cm^{-1}, H_2O molecules arise from the zinc(II) salts and it was also observed in the crystal structure of [Zn(II)(Tpy)(Pydc)·$4H_2O$] [18]. Other characteristic absorption bands such as ν(C=O) and ν(C=N) shifted to lower region on the complex,

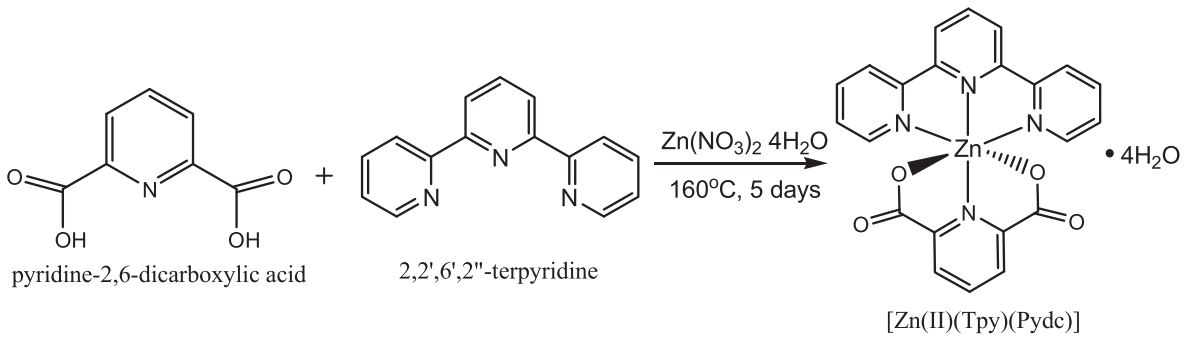

Scheme 1. Synthesis of [Zn(II)(Tpy)(Pydc)·$4H_2O$].

[Zn(II)(Tpy)(Pydc)·4H_2O], spectrum due to coordination with zinc(II) ion [19,20]. New bands at 516–553 cm^{-1} in the crystal give inference about ν(M–O) and ν(M–N) bonding.

3.2. Crystal structure of [Zn(II)(Tpy)(Pydc)·4H_2O]

In the complex [Zn(II)(Tpy)(Pydc)·4H_2O], Zn(II) is co-ordinated to both 2,2′:6′,2″-terpyridine and pyridine-2,6-dicarboxylate (Fig. 2). The structure of the compound showed an octahedral geometry with N(1A)N(12A)N(13A) N(27A)O(19A)O(30A) and N(1B)N(12B)N(13B)N(27B) O(19B)O(30B) planes from the two molecules bisecting each other at an angle of 33.35°. In both crystal structural compounds, the Zn(II) atom is coordinated to four nitrogen atoms (ZnA–N27A, ZnA–N12A, ZnA–N1A, and ZnA–N13A) with a bond distance ranging from 1.335 to 2.173 Å, comparable with the range usually observed in Zn(II) compounds with similar coordination mode [16]. The two carboxylate oxygen coordinated to the zinc(II) ion via Zn1A–O30A and Zn1A–O19A with bond distances of 2.179 and 2.213 Å, respectively. Four water molecules were found for each zinc(II) compound and are held by intermolecular hydrogen bond of the type O–H–O. The bond angles N27A–Zn1A–N12A, N27A–Zn1A–O30A, N12A–Zn1A–O30A, N27A–Zn1A–N1A, N12A–Zn1A–N1A, and O30A–ZnN1A are ranged within 90°–180° and are in accordance with the results obtained for octahedral complexes [16]. The complete crystallographic data and the structure refinement parameters are summarized in Table 1. Selected bond distances and angles (Å) for [Zn(II)(Tpy)(Pydc)·4H_2O] are given in Table 2.

The structure of the compound [Zn(II)(Tpy)(Pydc)·4H_2O] confirms that the compounds are held together by hydrogen bonding (Fig. 3) linking the crystallographically independent A and B molecules via water bridges, O–O distances are between 2.73 and 2.83 Å. These layers pack with minimal interdigitation (Fig. 4). A space volume of 292.52 $Å^3$ was observed.

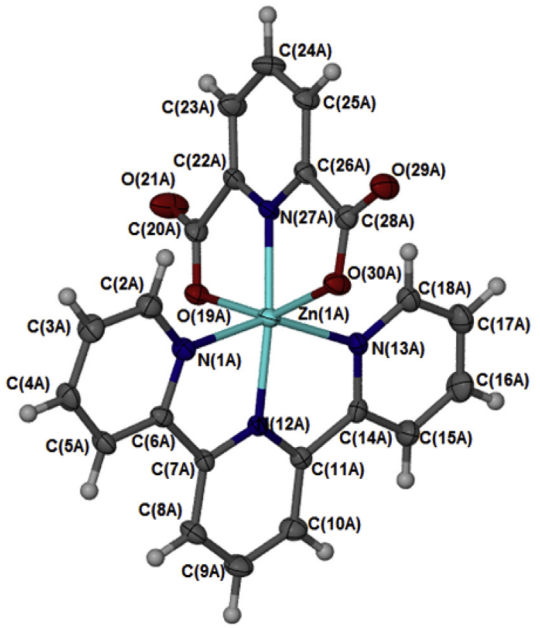

Fig. 2. An Oak Ridge Thermal Ellipsoid Plot (ORTEP) view of [Zn(II)(Tpy)(Pydc)·4H_2O] with ellipsoids drawn at 50% probability level. One of the two independent molecules is shown here; the other molecule has atomic labels ending B.

3.3. Thermogravimetric analysis

TGA of zinc(II) complex, [Zn(II)(Tpy)(Pydc)·4H_2O], is presented in Fig. 5. A seven-step decomposition pattern was observed for the complex, [Zn(II)(Tpy)(Pydc)·4H_2O]. An 8% weight loss was clearly observed around 81 °C, this was immediately followed by a gradual weight loss of 4% up to 288 °C. All water molecules (calculated for the unit) were lost in the temperature range between 81 and 288 °C (obsd 13.4%, calcd 12.0%). The decomposition of co-ordinated ligands 2,2′:6′,2″-terpyridine (Tpy) and pyridine-2,6-dicarboxylic acid (Pydc) was observed to begin at 290 °C with successive weight losses of 10%, 4%, 15%, and 10% at 312, 336, 357, and 448 °C, respectively. The final weight loss of 35% resulted in the formation of zinc oxide (~15%) at 552 °C. TGA plots of ligands, 2,2′:6′,2″-terpyridine (Tpy) and pyridine-2,6-dicarboxylate (Pydc), are presented in Supplementary data (Figs. S2 and S3).

3.4. Luminescence properties

Luminescence emission spectra of 2,2′:6′,2″-terpyridine, pyridine-2,6-dicarboxylic acid, and [Zn(II)(Tpy)(Pydc)·4H_2O] were obtained in DMSO at room temperature as shown in Fig. 6. 2,2′:6′,2″-Terpyridine and pyridine-2,6-dicarboxylic acid exhibited blue fluorescent emission bands at 424 nm (λ_{ex} = 330) and 489 nm (λ_{ex} = 346), respectively. Emissions at these wavelengths are assigned to intraligand ($\pi \rightarrow \pi^*$) transition [20,21]. A second weak emission band for pyridine-2,6-dicarboxylic acid at 372 nm was attributable to $n \rightarrow \pi^*$ transition. Shifts in the emission wavelengths were observed for [Zn(II)(Tpy)(Pydc)·4H_2O] at 412 and 434 nm (λ_{ex} = 346) when compared with those of the free ligands, this was ascribed to coordination of the Zn(II) with nitrogen and oxygen donor atoms of 2,2′:6′,2″-terpyridine and pyridine-2,6-dicarboxylic acid (metal-to-ligand charge transfer). The UV spectra (λ_{ex} = 346) in DMSO indicate that the solid-state octahedral geometry of [Zn(II)(Tpy)(Pydc)·4H_2O] is preserved in solution. The luminescent emission of [Zn(II)(Tpy)(Pydc)·4H_2O] indicates that it may be a potential compound for optical and blue-light emitting materials. These findings are in good agreement with our previous study on Zn(II)-related complexes [22].

3.5. Hirshfeld surface analyses

The molecular Hirshfeld surface [23] (d_{norm}, curvedness, and shape index for [Zn(II)(Tpy)(Pydc)·4H_2O]) is demonstrated in Fig. 4 and mapped over d_{norm} ranges −0.3346 to 1.4318 Å, shape index ranges −0.9993 to 0.9977 Å, and curvedness ranges −4.5383 to 0.8944 Å. The d_{norm} mapping indicates the strong hydrogen bond interactions, such as O–H···O hydrogen bonding between coordinated/lattice water and carboxylate oxygen, which gives the indication

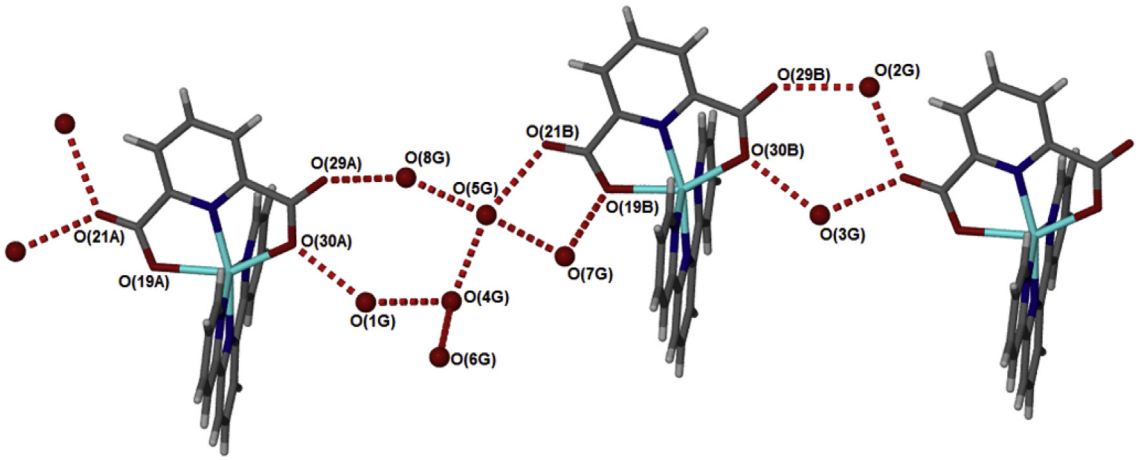

Fig. 3. Hydrogen bonds connect the water guest molecules to alternating A and B molecules of [Zn(II)(Tpy)(Pydc)·4H_2O].

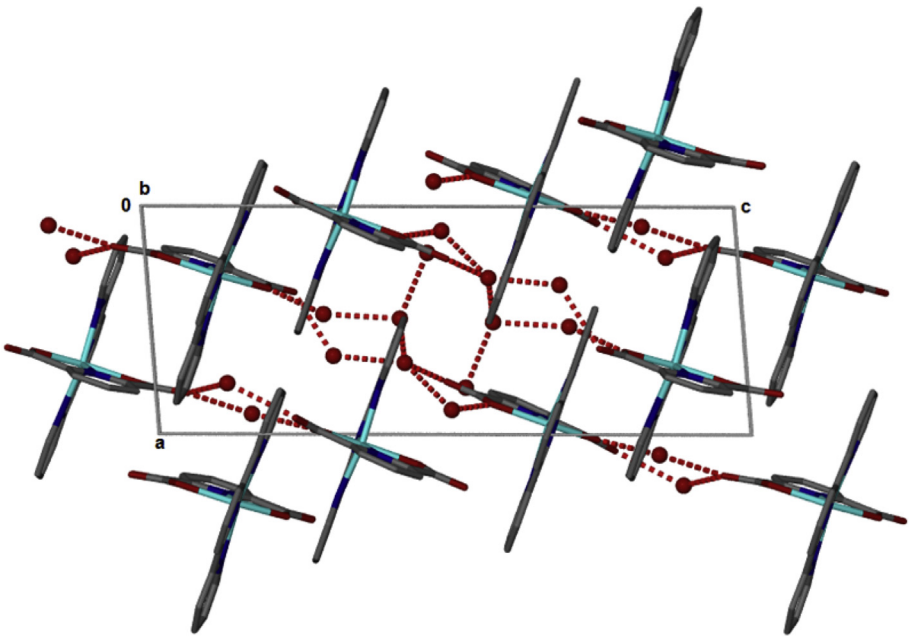

Fig. 4. Packing in [Zn(II)(Tpy)(Pydc)·4H_2O].

that the main interaction between complexes occurs around the region seen as a bright red area in the Hirshfeld surface area (Fig. 7). The two-dimensional fingerprint plots for [Zn(II)(Tpy)(Pydc)·4H_2O] (Fig. 8) show that the intermolecular H···H, O—H···O, and C—H···π interactions are well dominated and are in complement to the Hirshfeld surface area.

Shit et al. [24] reported that the shape index is the most sensitive to very subtle changes in surface shape, the red triangles on them (above the plane of the molecule) are represented by the concave regions indicating atoms of the π-stacked molecule above them, and the blue triangles are represented by the convex regions indicating the ring atoms of the molecule inside the surfaces [24]. The measure of the shape of the surface area of [Zn(II)(Tpy)(Pydc)·4H_2O] is defined by the curvedness [24]. The flat areas of the surface correspond to low values of curvedness, whereas sharp curvature areas correspond to high values of curvedness and usually tend to divide the surface into patches, indicating interactions between neighboring molecules. The large flat region, which is demarcated by a light blue outline, refers to the π···π stacking interactions. Two sharp spikes pointing toward lower left of the plot are typical O—H···O hydrogen bonds. This portion corresponds to O—H/H—O interactions comprising 46.0% of the total Hirshfeld surface area for [Zn(II)(Tpy)(Pydc)·4H_2O]. C—H···π interactions were observed in the fingerprint plots of H—C/C—H contacts

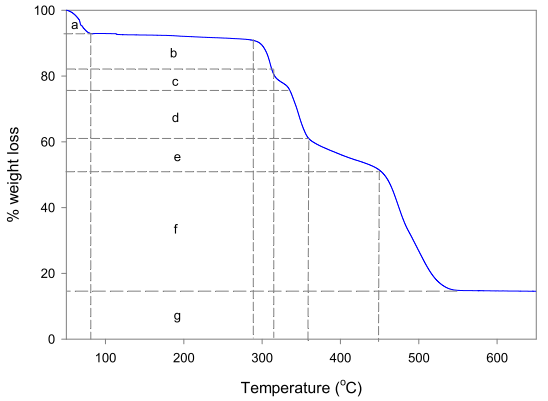

Fig. 5. TGA plot of [Zn(II)(Tpy)(Pydc)·4H_2O], where a = 8% wt. loss (Temp = 81 °C); b = 4% wt. loss (Temp = 288 °C); c = 10% wt. loss (Temp = 312 °C); d = 4% wt. loss (Temp = 336 °C); e = 15% wt. loss (Temp = 357 °C); f = 10% wt. loss (Temp = 448 °C) and g = 15% wt. loss (Temp = 552 °C).

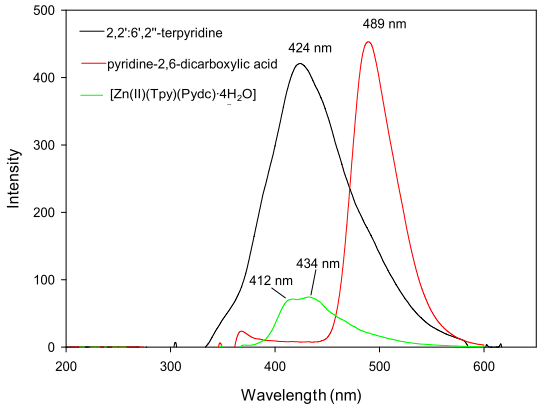

Fig. 6. Emission spectra of 2,2′:6′,2″-terpyridine, pyridine-2,6-dicarboxylic acid, and [Zn(II)(Tpy)(Pydc)·4H_2O].

comprising 12.1% of the total Hirshfeld surface area for [Zn(II)(Tpy)(Pydc)·4H_2O]. They correspond to all C—H···C interactions of which C—H···π appears in the same fingerprint plot. The broad region bearing short and narrow spikes at the middle of the plot is reflected as H···H interaction in [Zn(II)(Tpy)(Pydc)·4H_2O] comprising 17.9% of the total Hirshfeld surface area for [Zn(II)(Tpy)(Pydc)·4H_2O]. Apart from these, the presence of C···O, O···O, C···C, N···H, and O···C less important interactions is observed and summarized in Table S1.

3.6. Interaction between [Zn(II)(Tpy)(Pydc)·4H_2O] and amoxicillin

To demonstrate the potential medical application of [Zn(II)(Tpy)(Pydc)·4H_2O], the interaction property between amoxicillin and [Zn(II)(Tpy)(Pydc)·4H_2O] was examined. Amoxicillin was chosen as it is widely used for bacterial *sinusitis*. This technique was used to quantify the amount of amoxicillin adsorbed into the [Zn(II)(Tpy)(Pydc)·4H_2O]. Interaction studies were ascertained using a UV—vis spectrophotometer at 256 nm (Fig. 9). Calibration curve obtained for amoxicillin solution at 256 nm is presented in Fig. S4. The complex, [Zn(II)(Tpy)(Pydc)·4H_2O], remained undissolved in amoxicillin solution (in H_2O) during the study.

About 97.5% of amoxicillin interacted with [Zn(II)(Tpy)(Pydc)·4H_2O] (Table 3). This was attributed to hydrogen bonding, C—H—π interaction, and electrostatic interaction at a molecular level between [Zn(II)(Tpy)(Pydc)·4H_2O] and amoxicillin.

To further illustrate this finding, theoretical studies on the electronic properties of [Zn(II)(Tpy)(Pydc)·4H_2O] were carried out.

3.7. Theoretical studies

Molecular interactions between [Zn(II)(Tpy)(Pydc)·4H_2O] and amoxicillin were modeled. HOMO and LUMO positions on amoxicillin are presented in Fig. 10. HOMO centers around the hydroxy phenolic ring of amoxicillin, whereas LUMO is located around heptane-24-carboxylic acid end of amoxicillin.

Zinc(II) complexes of 2,2′:6′,2″-terpyridine and pyridine-2,6-dicarboxylic acid, [Zn(II)(Tpy)(Pydc)·4H_2O], showed HOMO centers around the metal center and pyridine-2,6-dicarboxylate group, whereas LUMO is situated around 2,2′:6′,2″-terpyridine ring (Fig. 11).

An adduct was formed when [Zn(II)(Tpy)(Pydc)·4H_2O] and amoxicillin were brought in contact with each other. In this, the HOMO position originates from the hydroxy phenolic ring of amoxicillin and LUMO is situated around the 2,2′:6′,2″-terpyridine ring of [Zn(II)(Tpy)(Pydc)·4H_2O] (Fig. 12a). This clearly indicated that the interaction between [Zn(II)(Tpy)(Pydc)·4H_2O] and amoxicillin is through electron transfer from the HOMO positions to LUMO atoms (Fig. 12b). Electron transfer further confirms the possibility of forming π—π interaction between aromatic rings of

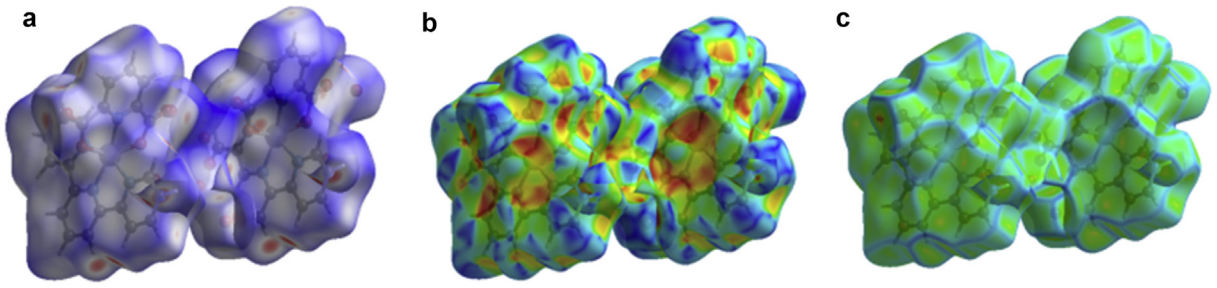

Fig. 7. Molecular Hirshfeld surface area: (a) d_{norm}, (b) shape index, and (c) curvedness for [Zn(II)(Tpy)(Pydc)·4H_2O].

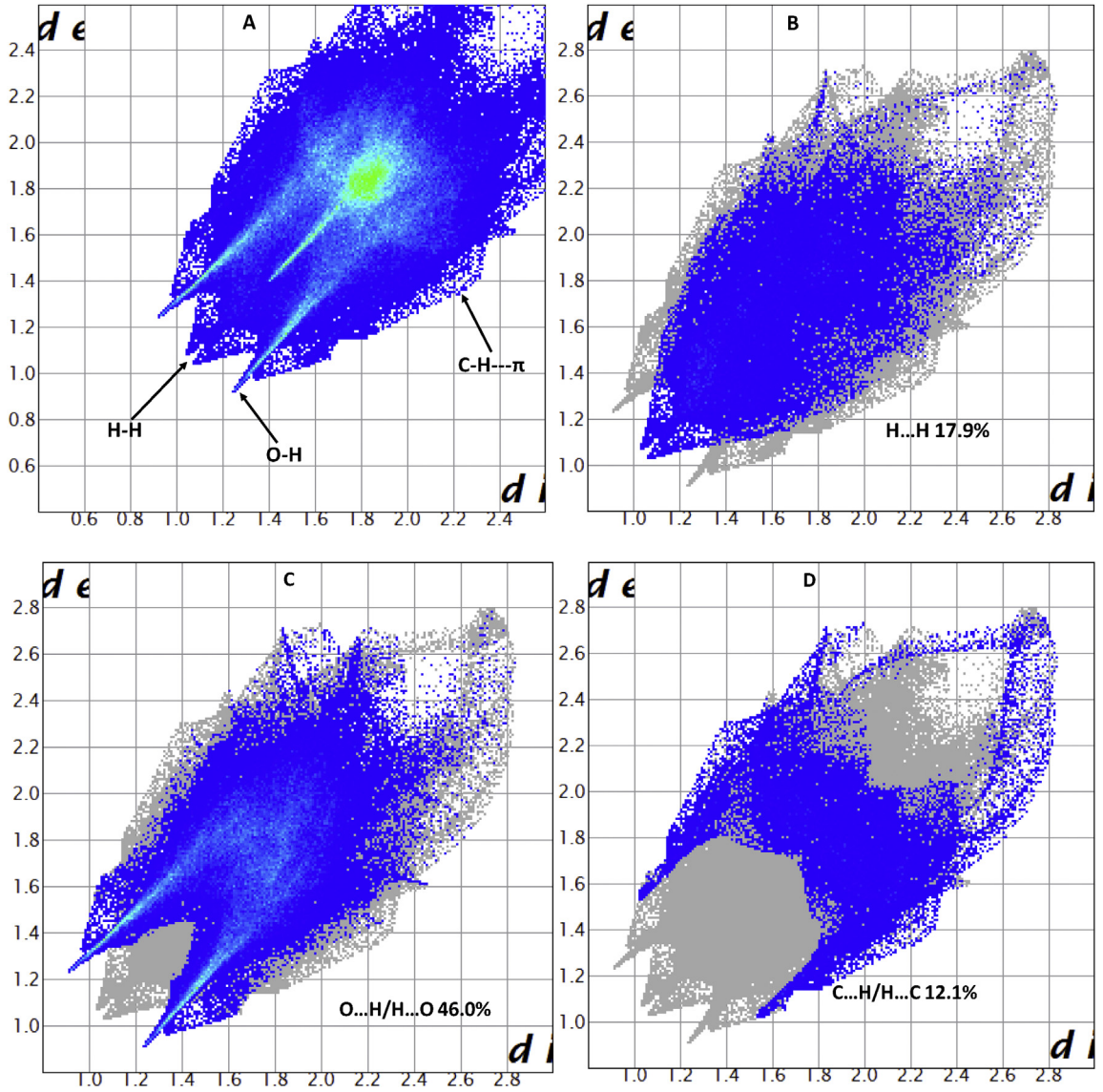

Fig. 8. Fingerprint plot of [Zn(II)(Tpy)(Pydc)·4H_2O]: (a) full and resolved into (b) H···H, (c) O–H/H–O, and (d) H···C contacts showing the percentages of contacts contributed to the total Hirshfeld surface area.

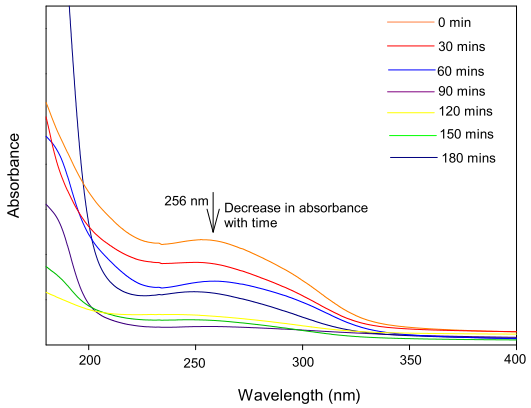

Fig. 9. UV spectra of amoxicillin dissolved in water showing absorbance decreases with time.

mostly terpyridine rings of [Zn(II)(Tpy)(Pydc)·4H_2O] and the hydroxy phenolic ring of amoxicillin.

3.7.1. Energy gap (ΔE)

The HOMO–LUMO gap describes the stability and resistance of molecules, and it also predicts activity

Table 3
Absorbance, concentration, percentage, and mass of amoxicillin before and after interaction with [Zn(II)(Tpy)(Pydc)·4H_2O] at 30 ± 2 °C.

Parameters	Before contact	After contact (filtration)
Absorbance of Amoxicillin	0.236	0.006
Concentration of amoxicillin	5.47×10^{-3} M	1.40×10^{-4} M
Percentage of amoxicillin	100%	2.50%

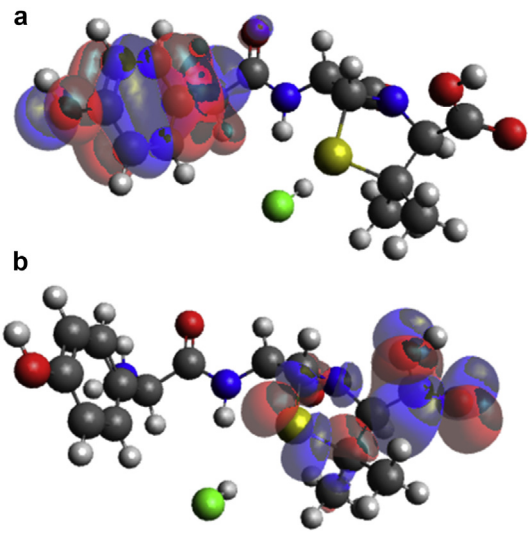

Fig. 10. (a) HOMO and (b) LUMO locations on modeled amoxicillin.

between species by providing the electrical transport properties as well as electron carrier and mobility in molecules [25]. HOMO and LUMO energies of amoxicillin, [Zn(II)(Tpy)(Pydc)·4H_2O], and [Zn(II)(Tpy)(Pydc)·4H_2O]–amoxicillin adduct are presented in Fig. 13. Low HOMO energy (better electron donor) describes the observed high ionization potential observed, whereas high LUMO energy (better electron acceptor) confirms high electron affinity. The energy gaps of amoxicillin, [Zn(II)(Tpy)(Pydc)·4H_2O], and [Zn(II) (Tpy) (Pydc)·4H_2O]–amoxicillin adduct were 4.945, 4.248 and 3.205 eV, respectively. The observed energy, 3.205 eV, is indicative of a favorable interaction between amoxicillin and [Zn(II)(Tpy)(Pydc)·4H_2O].

3.7.2. *Electrostatic charge transfer*

The charge transfer was investigated by natural bond orbital analysis by looking at the partial charge difference in amoxicillin, [Zn(II) (Tpy) (Pydc)·4H_2O], and [Zn(II) (Tpy) (Pydc)·4H_2O]–amoxicillin adduct before and after the interaction. Some atomic partial charges on atoms of amoxicillin were observed to shift slightly after the formation of adduct, thus further indicating that charge

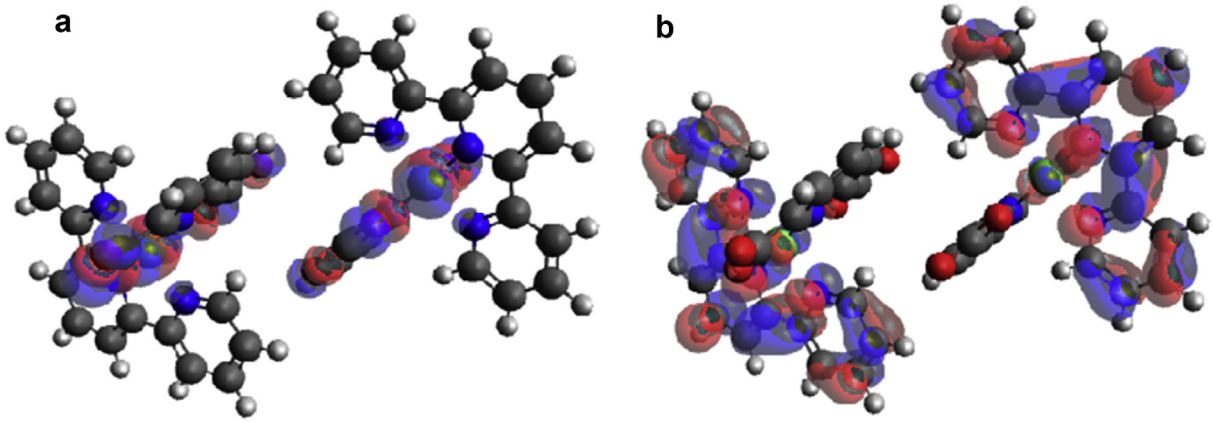

Fig. 11. (a) HOMO and (b) LUMO locations on modeled [Zn(II)(Tpy)(Pydc)·4H_2O].

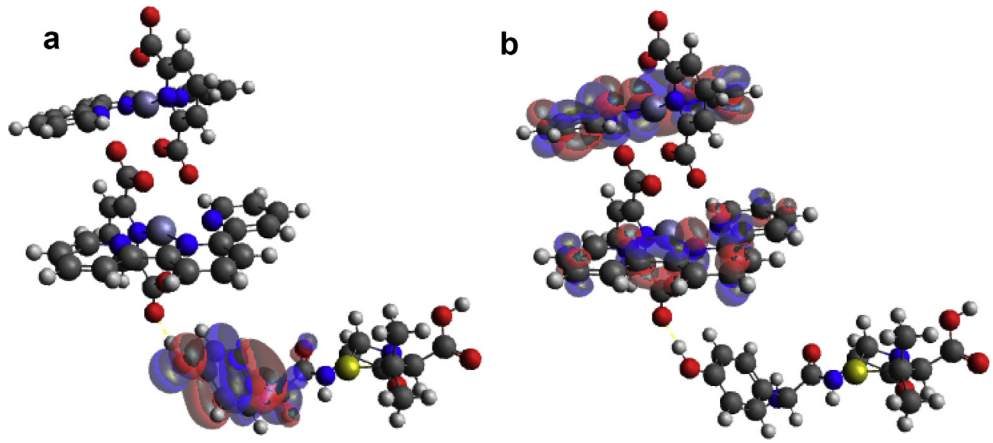

Fig. 12. (a) HOMO and (b) LUMO locations on modeled [Zn(II)(Tpy)(Pydc)·4H_2O]–amoxicillin adduct.

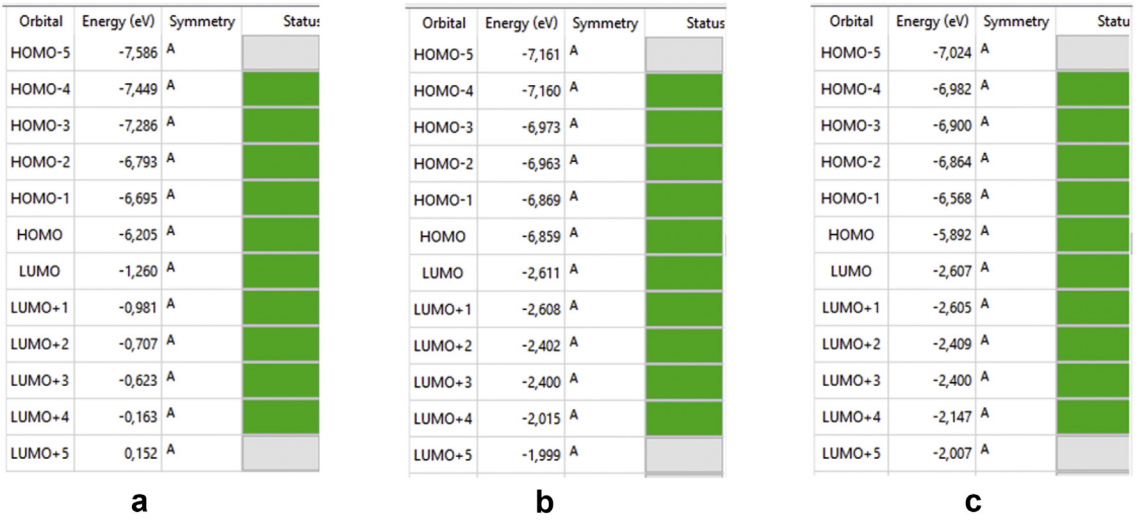

Orbital	Energy (eV)	Symmetry	Status
HOMO-5	-7,586	A	
HOMO-4	-7,449	A	
HOMO-3	-7,286	A	
HOMO-2	-6,793	A	
HOMO-1	-6,695	A	
HOMO	-6,205	A	
LUMO	-1,260	A	
LUMO+1	-0,981	A	
LUMO+2	-0,707	A	
LUMO+3	-0,623	A	
LUMO+4	-0,163	A	
LUMO+5	0,152	A	

a

Orbital	Energy (eV)	Symmetry	Status
HOMO-5	-7,161	A	
HOMO-4	-7,160	A	
HOMO-3	-6,973	A	
HOMO-2	-6,963	A	
HOMO-1	-6,869	A	
HOMO	-6,859	A	
LUMO	-2,611	A	
LUMO+1	-2,608	A	
LUMO+2	-2,402	A	
LUMO+3	-2,400	A	
LUMO+4	-2,015	A	
LUMO+5	-1,999	A	

b

Orbital	Energy (eV)	Symmetry	Statu
HOMO-5	-7,024	A	
HOMO-4	-6,982	A	
HOMO-3	-6,900	A	
HOMO-2	-6,864	A	
HOMO-1	-6,568	A	
HOMO	-5,892	A	
LUMO	-2,607	A	
LUMO+1	-2,605	A	
LUMO+2	-2,409	A	
LUMO+3	-2,400	A	
LUMO+4	-2,147	A	
LUMO+5	-2,007	A	

c

Fig. 13. HOMO and LUMO energies of (a) amoxicillin, (b) [Zn(II)(Tpy)(Pydc)·4H_2O], and (c) [Zn(II)(Tpy)(Pydc)·4H_2O]–amoxicillin adduct.

transfer occurs from amoxicillin to [Zn(II)(Tpy)(Pydc)·4H_2O].

Partial charges on sulfur (S), oxygen (from –OH), oxygen (from –COOH), and nitrogen (on amoxicillin) before interaction with [Zn(II)(Tpy)(Pydc)·4H_2O] were 0.081, −0.757, −0.741, and (−0.530, −0.671, −0.944), respectively. After interaction with [Zn(II)(Ter)(Pydc)·4H_2O] to form an adduct, new partial charges on sulfur (S), oxygen (from –OH), oxygen (from –COOH), and nitrogen (on amoxicillin) were 0.099, −0.795, −0.738, and (−0.527, −0.943, −0.673), respectively. This confirms the transfer of electron from amoxicillin to [Zn(II)(Tpy)(Pydc)·4H_2O] for adduct formation to take place.

Oxygen atoms on [Zn(II)(Tpy)(Pydc)·4H_2O] before and after the interaction with amoxicillin were (−0.815, −0.812, −0.753, −0.747) and (−0.816, −0.771, −0.757, −0.747), respectively. A slight change was also observed with nitrogen atoms with partial charges becoming less negatively charged upon forming adduct. The zinc(II) ion becomes more positively charged upon forming adduct (from 1.363 to 1.377).

Electronic identifiers calculated indicated that amoxicillin is slightly softer than [Zn(II)(Tpy)(Pydc)·4H_2O] and vice versa with hardness, notwithstanding within close range. Complex, [Zn(II)(Tpy)(Pydc)·4H_2O], is highly electronegative as compared with amoxicillin, thus attracting electron from amoxicillin for adduct formation to take place (Table 4).

Table 4
Some electronic structure identifiers of the studied adducts.

Parameters	Amoxicillin	[Zn(II)(Tpy)(Pydc)·4H_2O]	Adduct
Hardness (η)	2.4725	2.124	1.6025
Softness (σ)	0.4044	0.4708	0.6240
Electronegativity (χ)	3.7325	4.7350	4.2495
Chemical potential (μ)	−3.7325	−4.7350	−4.2495

3.7.3. Electronic properties (UV adsorption analysis)

The electronic properties of [Zn(II)(Tpy)(Pydc)·4H_2O], amoxicillin, and adduct were calculated using the time-dependent density functional theory (TD-DFT) approach on the previously optimized ground-state compounds in the gas phase (Fig. S5). The excitation wavelengths (λ) of [Zn(II)(Tpy)(Pydc)·4H_2O], amoxicillin, and adduct were 334, 268, and 551 nm, respectively. The observed shift in wavelength confirmed the formation of adducts.

4. Conclusions

We have reported the synthesis of a novel complex [Zn(II)(Tpy)(Pydc)·4H_2O] via a solvothermal method. X-ray crystallography confirmed the formation of octahedral zinc(II) complex of 2,2′:6′,2″-terpyridine (Ter) and pyridine-2,6-dicarboxylic acid (Pydc), [Zn(II)(Tpy)(Pydc)·4H_2O]. Luminescent emission of [Zn(II)(Tpy)(Pydc)·4H_2O] indicated that the complex may have potential application as sensors for optical and blue–light emitting materials. Structural characterization of [Zn(II)(Tpy)(Pydc)·4H_2O] revealed that the net supramolecular arrangements are dictated by H···H, O···H, and C–H···π interactions. Experimental and theoretical studies clearly indicated that [Zn(II)(Tpy)(Pydc)·4H_2O] dimer interacts with amoxicillin via electron transfer, π–π interaction, hydrogen bond interaction, and van der Waals forces. The observed interaction between [Zn(II)(Tpy)(Pydc)·4H_2O] and amoxicillin shows possible development of the complex for medicinal applications.

Acknowledgments

M.D.O. acknowledges financial support from the Organization for Women in Science for the Developing World (OWSD). The authors thank the Centre for High Performance Computing (CHPC), Cape Town, South Africa for providing the platform in carrying out the molecular modeling studies on the Gaussian09 software.

Appendix A. Supplementary data

Supplementary data to this article can be found online at https://doi.org/10.1016/j.crci.2018.11.007.

References

[1] G.L. Eichhorn, L.G. Marzilli, Advances in Inorganic Biochemistry Models in Inorganic Chemistry, PTR Prentice-Hall, Inc, New Jersey, 1994.
[2] M.N. Hughes, The Inorganic Chemistry of Biological Processes, 2nd ed., Wiley, Chichester [England], 1984.
[3] M.H. Tarafder, N. Saravanan, K.A. Crouse, A.M. Ali, Transit. Met. Chem. 26 (2001) 613–618.
[4] Y. Ali Mohammed, T. Baraki, R.K. Upadhyay, A. Masood, Am. J. Appl. Chem. 2 (2014) 15–18.
[5] H. Singh, A.K. Varshney, Bioinorg. Chem. Appl. 23245 (2006) 1–7.
[6] A.S. Shayma, F. Yang, A. Abbas Salleh, Eur. J. Sci. Res. 33 (2009) 702–709.
[7] Y. Ali Mohammed, Asian Med. J. 2 (2015) 14–25.
[8] M.N. Hughes, Inorganic Chemistry of Biological Processes, Wiley, New York, 1981. Mir, Moscow, 1983.
[9] S.V. Lapshin, V.G. Alekseev, Russ. J. Inorg. Chem. 54 (2009) 1066–1069.
[10] A.P. Avtsin, A.A. Zhavoronkov, M.A. Rish, L.S. Strochkova, Human Microelementoses, Meditsina, Moscow, 1991, p. 496.
[11] A. Zarkan, H.-R. Macklyne, D.Y. Chirgadze, A.D. Bond, A.R. Hesketh, H.-J. Hong, Sci. Rep. 7 (2017) 4893.
[12] G.M. Sheldrick, Acta Crystallogr. A64 (2008) 112–122.
[13] M.J. Frisch, G.W. Trucks, H.B. Schlegel, G.E. Scuseria, M.A. Robb, J.R. Cheeseman, G. Scalmani, V. Barone, B. Mennucci, G.A. Petersson, H. Nakatsuji, M. Caricato, X. Li, H.P. Hratchian, A.F. Izmaylov, J. Bloino, G. Zheng, J.L. Sonnenberg, M. Hada, M. Ehara, K. Toyota, R. Fukuda, J. Hasegawa, M. Ishida, T. Nakajima, Y. Honda, O. Kitao, H. Nakai, T. Vreven, J.A. Montgomery Jr., J.E. Peralta, F. Ogliaro, M. Bearpark, J.J. Heyd, E. Brothers, K.N. Kudin, V.N. Staroverov, R. Kobayashi, J. Normand, K. Raghavachari, A. Rendell, J.C. Burant, S.S. Iyengar, J. Tomasi, M. Cossi, N. Rega, J.M. Millam, M. Klene, J.E. Knox, J.B. Cross, V. Bakken, C. Adamo, J. Jaramillo, R. Gomperts, R.E. Stratmann, O. Yazyev, A.J. Austin, R. Cammi, C. Pomelli, J.W. Ochterski, R.L. Martin, K. Morokuma, V.G. Zakrzewski, G.A. Voth, P. Salvador, J.J. Dannenberg, S. Dapprich, A.D. Daniels, Ö. Farkas, J.B. Foresman, J.V. Ortiz, J. Cioslowski, D.J. Fox, Gaussian 09 Software, Gaussian, Inc., Wallingford, CT, 2009.
[14] S.G. Zhang, W. Lei, M.Z. Xia, F.Y. Wang, J. Mol. Struct. 732 (2005) 175–182.
[15] M. Lashgari, M.R. Arshadi, G.A. Parsafar, Corros. Sci. 61 (2005) 778–783.
[16] T. Dudev, C. Lim, J. Am. Chem. Soc. 122 (2000) 11146–11153.
[17] A.C. Tella, S. O Owalude, P.A. Ajibade, N. Simon, S.J. Olatunji, M.S. Adbelbaky, S. Garcia-granda, J. Mol. Struct. 1125 (2016) 570–575.
[18] H.G. Jin, Y.Z. Yan, J. Li, Z.G. Gu, J.H. Chen, Y.T. Liu, Z.P. Zheng, Q.G. Zhan, Y.P. Cai, Inorg. Chem. Commun. 23 (2012) 25–30.
[19] A.C. Tella, A.C. Oladipo, O.G. Adeyemi, O.S. Oluwafemi, S.O. Oguntoye, L.O. Alimi, J.T. Ajayi, S.K. Degni, Solid State Sci. 68 (2017) 1–9.
[20] Z. Kucukbay, H. Yazlak, N. Sahin, M. Tuzcu, M.N. Cakmak, F. Gurdogan, V. Juturu, K. Sahin, Aquaculture 257 (2006) 465–469.
[21] T. Yutaka, S. Obara, S. Ogawa, K. Nozaki, N. Ikeda, T. Ohno, Y. Ishii, K. Sakai, M. Haga, Inorg. Chem. 44 (2005) 4737–4746.
[22] A.C. Tella, S.O. Owalude, M.F. Omotoso, S.J. Olatunji, A.S. Ogunlaja, L.O. Alimi, O.K. Popoola, S.A. Bourne, J. Mol. Struct. 1157 (2018) 450–456.
[23] M.J. Turner, J.J. McKinnon, S.K. Wolff, D.J. Grimwood, P.R. Spackman, D. Jayatilaka, M.A. Spackman, CrystalExplorer, vol. 17, University of Western Australia, Perth, 2017.
[24] S. Shit, C. Marschner, S. Mitra, Acta Chim. Slov. 63 (2016) 129–137.
[25] A.S. Ogunlaja, E. Hosten, Z.R. Tshentu, Ind. Eng. Chem. Res. 53 (2014) 18390–18401.